Detection Performance using Frequency Diversity with Distributed Sensors

BYUNG WOOK JUNG, Student Member, IEEE
KAIST

RAVIRAJ S. ADVE, Senior Member, IEEE
University of Toronto

JOOHWAN CHUN, Senior Member, IEEE
KAIST

MICHAEL C. WICKS, Fellow, IEEE
Air Force Research Laboratory

Detection using a frequency diverse (FD), distributed, radar system is investigated. Distributed sensing systems provide an inherent spatial diversity by viewing a potential target from different aspect angles. By using different frequencies at each platform, a diversity gain is obtained in addition to the advantages of spatial diversity while also avoiding mutual interference. Here, since platforms are distributed spatially, true time delay is used at each platform to align the sample look point in time. Data models for a distributed system with and without frequency diversity are developed. These models are used to analyze the corresponding signal-to-interference-plus-noise ratio (SINR) and probability of detection for the two cases in the context of space-time adaptive processing (STAP). The simulation results presented here illustrate the limitations imposed by mutual interference and the significant benefits of spatial and frequency diversity.

Manuscript received October 15, 2009; revised March 12, 2010; released for publication June 15, 2010.

IEEE Log No. T-AES/47/3/941764.

Refereeing of this contribution was handled by Y. Abramovich.

The work of B. W. Jung and J. Chun was supported under a contract from Samsung Thales Co.

Authors' addresses: B. W. Jung and J. Chun, Dept. of Electrical Engineering, KAIST, 335 Gwahak-ro, Yuseong-gu, Daejeon, 305-701, Republic of Korea; R. S. Adve, Dept. of Electrical and Computer Engineering, University of Toronto, 10 King's College Road, Toronto, ON, Canada M5S 3G4, E-mail: (rsadve@comm.utoronto.ca); M. C. Wicks, Air Force Research Laboratory, 26 Electronic Parkway, Rome, NY 13441-4514.

I. INTRODUCTION

Distributed RF sensing systems have been an active research area for some time now [1–5]. In spite of the increased complexity due to its distributed configuration, such a system has many advantages: energy from a target echo generated by one platform can be used by many platforms, which reduces the energy necessary for the coverage of a large surveillance volume; the observations from the different aspect angles reduce the probability of miss yielding an antistealth characteristic, especially with fluctuating targets. This spatial diversity is the main advantage of a distributed sensing system; the reader is referred to [1], [2] for a more detailed discussion of the benefits of distributed systems.

Most of the original work in distributed RF sensing, or multistatic radar, focused on the simplest case of a single transmitter and multiple receivers [3–6]. This simplest configuration is extended multiple transmitters and multiple receivers. This system is analyzed preliminarily in [1]. Recently Fischler et al. proposed a detector improving detection performance under the system with multiple transmitter and multiple receivers [7]. In [8] the authors generalize this configuration allowing for multiple colocated antennas at each platform, i.e., an antenna array at each transmitter/receiver. This paper focuses on this most general configuration that includes the first and second configurations as special cases. In this regard, a recent proposal has been the use of frequency diversity to allow for the simultaneous processing of multiple transmit-receive pairs [9]. This approach is one, but not the only, implementation of a multiple-input multiple-output (MIMO) radar wherein multiple distributed transmitters radiate waveforms orthogonal in some convenient dimension [10].

A related track in radar signal processing is that of interference suppression. Radar systems, especially airborne systems, invariably deal with strong interference. Space-time adaptive processing (STAP) techniques promise to be the best means to detect weak signals in severe, dynamic, interference scenarios including clutter and electromagnetic interference (EMI) [11, 12]. STAP entails adaptively combining signals received at multiple antenna elements and over multiple pulses within a single coherent pulse interval (CPI). While STAP was originally developed for monostatic radar, it has been recently extended to bistatic [13, 14] and multistatic configurations [8, 9, 15].

A crucial issue raised in [9] is that joint adaptive processing across multiple platforms requires true time delay to align, in time, the signals received at the multiple transmit-receive pairs. The system in [9] is a ground-based system with a single antenna at each radar platform. Using true time delay, each platform can process target signals from multiple transmissions simultaneously. However, a significant overhead is that such a system allows for probing only a single look point in space. This is in contrast to a monostatic STAP system where a look direction is probed [12]. Such a system is therefore best used after preliminary processing has identified a few regions of interest. Since the true time delay allows focusing at a single point (point target) in space, an adaptively combined signal provides robust detection as well as improved track-while-scan accuracy.

This paper investigates STAP for airborne distributed sensor systems. Our system is closest in design to the work in [15] wherein the authors derive the likelihood ratio test and investigate distributed detection for such a system of radars, comparing optimal and decentralized detection. There are however, some important differences: in [15], the authors assume each platform receives only a single signal, whereas multiple transmissions from different platform are considered in this paper. Here we consider, in some detail, the issues that would arise in implementing STAP algorithms in a distributed radar such as multiple, simultaneous, illuminating sources and true time delay. Furthermore, the authors use a proxy for signal-to-interference-plus-noise ratio (SINR) whereas here we use a more traditional definition of SINR. Finally, while there is some conceptual overlap in the discussion of probability of detection (P_D), the systems under consideration are different enough to warrant our discussion.

The contributions of this paper are:

1) the development of a data model for distributed radar networks with and without frequency diversity extending the true time delay model of [9] and the bistatic radar model of [16], [17],

2) the analysis of both cases using SINR and probability of detection as figures of merit, in turn illustrating the importance of frequency diversity,

3) numerical simulations implementing the data model to illustrate the robustness provided by spatial and frequency diversity and the importance of avoiding mutual interference across platforms.

Notation: In this paper, scalars are denoted in italics, e.g., x, vectors are denoted in bold face, lowercase letters, e.g., $\mathbf{x}$, while matrices are denoted in bold face, upper case letters, e.g., $\mathbf{R}$. $\mathbf{I}_N$ represents the $N \times N$ identity matrix and $\mathrm{E}\{\cdot\}$ represents the statistical expectation operator. Spatial and velocity vectors in 3-dimensional space, on the other hand, are denoted with an overline, e.g., $\bar{v}$.

The remainder of this paper is organized as follows. Section II presents the system model for the distributed sensor system under consideration, developing both the case with and without frequency diversity. The data models for the desired signal, clutter and noise are developed in Section III. Section IV presents the analysis of the systems in terms of SINR and P_D. The analysis is accompanied by results of simulations to illustrate the performance gains due to spatial and frequency diversity in distributed RF sensor systems. This paper ends in Section V after drawing some conclusions and indicating potential avenues for future research.

II. SYSTEM MODEL

This section develops the system model for a radar system with K distributed airborne apertures potentially using joint processing of the received signals over all K platforms. The entire system is used to detect the potential presence of a target in a specific region of space, the look point, and at a specific velocity, the look velocity. Each radar in the system transmits a pulse which reflects off the ground (causing clutter) and possibly a target. External sources of EMI may also be present. Unlike in [15], each platform receives the reflections due to its own transmissions and those of all other $K-1$ radars.

We distinguish two forms of this system: in the nonfrequency diverse (NFD) case, all platforms use the same center frequency f_0. Since the transmissions are concurrent, individual receptions cannot be isolated. In the frequency diverse (FD) case, each platform transmits at a different center frequency and, using bandpass filters (BPFs), each component of the received signal can be isolated.[1] Fig. 1 illustrates the workings of each of these forms of multistatic radar. In the figure $\mathbf{x}_{pq}$ represents the signal created at platform p due to a transmission from platform q. Note that for convenience, the figure presents only a single antenna at each element, though each platform uses N antenna elements and M pulses within a CPI, i.e., $\mathbf{x}_{pq}$ is a length-NM vector.

A. True Time Delay on Receive

In a system as illustrated above, an important issue for coherent processing is synchronization across platforms. Specifically, in order to probe the same look point from different angles and distances, the K radar apertures need to be synchronized. Furthermore, with potentially joint processing of the signals received at the K arrays, the samples at the receiver, which correspond to a specific range, need to be aligned in time. While distributed synchronization is outside the scope of this paper, the received samples are aligned using true time delays in relation to the look point [9]. The sample corresponding to the look point is therefore, effectively, sampled simultaneously by all receivers. The time delay, before sampling, used

[1] An alternative approach is to consider a system based on orthogonal frequency division multiple access (OFDMA) with the attendant reduction in hardware complexity, though potentially at a higher sampling rate [18].

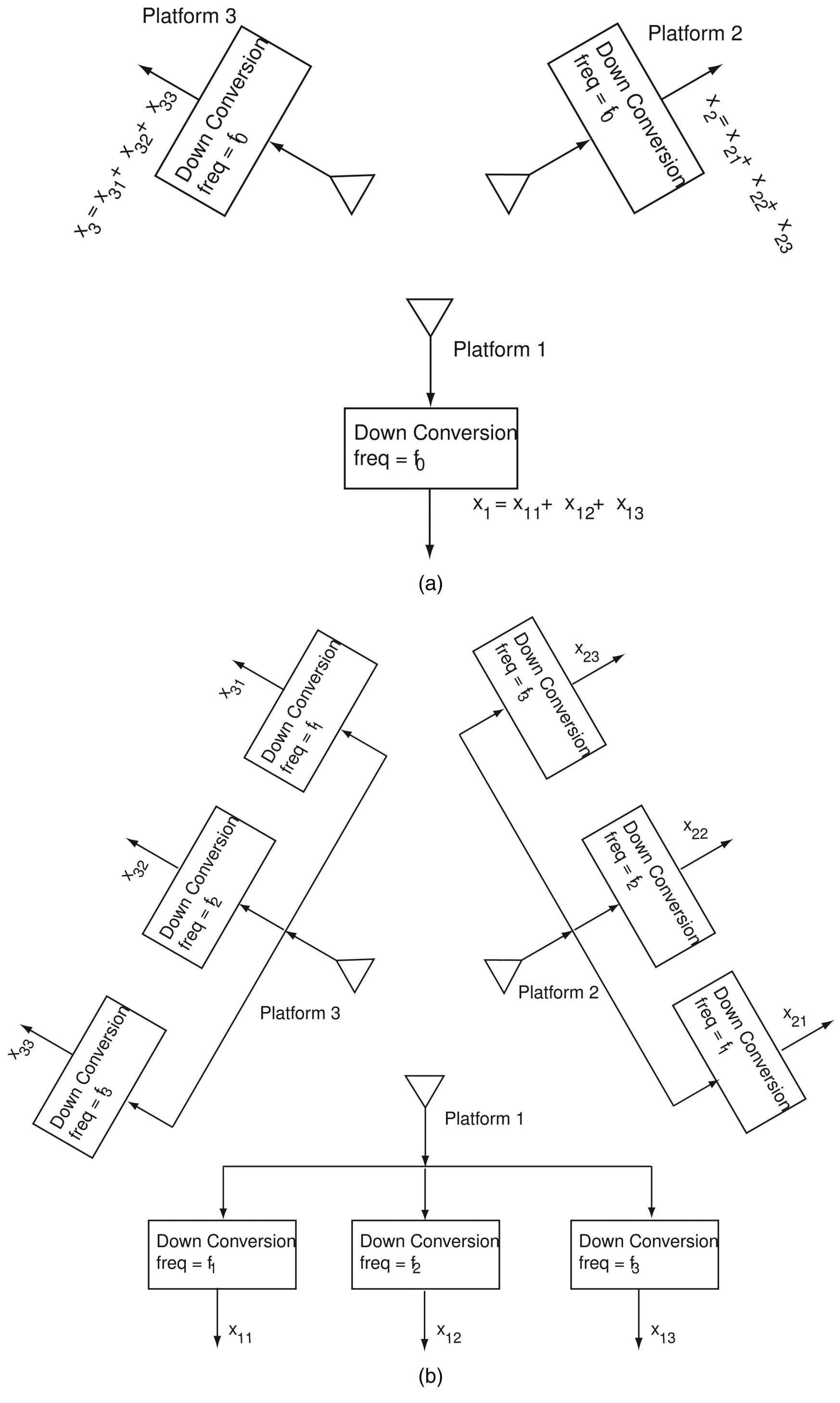

Fig. 1. Receiver structure without and with frequency diversity, respectively. (a) NFD case, $K = 3$. (b) FD case, $K = 3$.

by the pth platform is

$$\Delta T_p = \frac{\max_p\{D_p\} - D_p}{c} \tag{1}$$

where D_p is the distance between the look point and pth platform and c is the speed of light.

B. Signal Models for NFD and FD Cases

Because of the differences in resolvability of individual signals, the FD and NFD cases require their own signal models. This section develops these models for the two cases. In addition, for use with STAP, we also develop corresponding covariance matrices. Since the sensor platforms are widely separated, we assume that the signals received at the platforms are statistically independent.

1) *NFD Case*: In the NFD case, all platforms share a single frequency. As illustrated in Fig. 1(a), signals from individual platforms cannot be

distinguished and so the received signal at platform p is the sum over all reflected signals. Therefore, for platform p, the received signal corresponding to the target-absent (H_0) and target-present (H_1) hypotheses are, respectively,

$$
\begin{aligned}
H_0: \quad \mathbf{x}_p &= \sum_{q=1}^{K} \mathbf{x}_{pq} = \sum_{q=1}^{K} \mathbf{c}_{pq} + \mathbf{n}_p = \sum_{q=1}^{K} [\mathbf{c}_{pq} + \bar{\mathbf{n}}_{pq}] \\
&= \mathbf{c}_p + \mathbf{n}_p \\
H_1: \quad \mathbf{x}_p &= \sum_{q=1}^{K} \mathbf{x}_{pq} = \sum_{q=1}^{K} [\alpha_{pq}\mathbf{g}_{pq} + \mathbf{c}_{pq}] + \mathbf{n}_p \\
&= \sum_{q=1}^{K} [\alpha_{pq}\mathbf{g}_{pq} + \mathbf{c}_{pq} + \bar{\mathbf{n}}_{pq}] \\
&= \sum_{q=1}^{K} \alpha_{pq}\mathbf{g}_{pq} + \mathbf{c}_p + \mathbf{n}_p \qquad (2)
\end{aligned}
$$

where $\mathbf{c}_{pq}$ represents the clutter vector at platform p due to the transmission from platform q and $\mathbf{c}_p$ and $\mathbf{n}_p$ represent the overall interference (clutter and EMI) and additive white Gaussian noise (AWGN) components at platform p, respectively. For convenience in defining an interference-plus-noise covariance matrix, a new noise term for each incoming signal from platform q to p is defined as $\bar{\mathbf{n}}_{pq} = (1/K)\mathbf{n}_p$. Under hypothesis H_1, α_{pq} and $\mathbf{g}_{pq}$ represent the target amplitude and space-time steering vector, corresponding to the look point and look Doppler, at platform p due to the transmission from platform q. The amplitude, α_{pq} is assumed to follow a Swerling-II model, i.e., a complex Gaussian distribution with zero mean and variance σ^2_{tpq} (referred to as σ^2_{tp} when $p = q$). Since all platforms operate at a single frequency, $\mathbf{x}_p$ is a length-NM vector.

The covariance matrix, at platform p, under H_0, is therefore given by the $NM \times NM$ matrix $\mathbf{R}_{pq} = E\{\mathbf{x}_{pq}\mathbf{x}^H_{pq}\}$ for zero mean, Gaussian and independent $\mathbf{x}_{pq}$. Since all platforms share the same frequency,

$$
\mathbf{R}_p = \mathbf{R}_{p1} + \mathbf{R}_{p2} + \cdots + \mathbf{R}_{pK}. \qquad (3)
$$

2) *FD Case*: In the FD case, platform q transmits at a center frequency of f_q. We assume that there is no overlap between the K transmissions and each platform, therefore, is able to separate the K signals, as illustrated in Fig. 1(b).

For platform p, the received signal corresponding to the signal transmitted from platform q, at frequency f_q, in the target-absent (H_0) and target-present (H_1) hypotheses are, respectively,

$$
\begin{aligned}
H_0: \quad \mathbf{x}_{pq} &= \mathbf{c}_{pq} + \mathbf{n}_{pq} \\
H_1: \quad \mathbf{x}_{pq} &= \alpha_{pq}\mathbf{g}_{pq} + \mathbf{c}_{pq} + \mathbf{n}_{pq}
\end{aligned} \qquad (4)
$$

where α_{pq} is the target amplitude, $\mathbf{g}_{pq}$ is the target space-time steering vector corresponding to the look point and look Doppler frequency, $\mathbf{c}_{pq}$ is the interference component, incorporating clutter and EMI, and $\mathbf{n}_{pq}$ is the AWGN component at platform p due to the transmission from platform q. Each of the K vectors, corresponding to the K transmitted frequencies, received at the pth platform are of length NM.

Since each transmission occupies its own frequency band, the covariance matrix at platform p, under H_0 is a $KMN \times KMN$ block diagonal matrix. The covariance matrix of pth platform in FD case can be expressed as

$$
\mathbf{R}_p = \begin{bmatrix} \mathbf{R}_{p1} & \mathbf{0} & \cdots & \mathbf{0} \\ \mathbf{0} & \mathbf{R}_{p2} & \cdots & \mathbf{0} \\ \vdots & \vdots & \ddots & \vdots \\ \mathbf{0} & \mathbf{0} & \cdots & \mathbf{R}_{pK} \end{bmatrix} \qquad (5)
$$

where each diagonal entry is a $NM \times NM$ matrix associated with the corresponding transmit frequency.[2]

III. DATA MODEL

The previous section developed the signal and covariance matrix model for the NFD and FD cases. This section develops the data model for multistatic radar. To focus on the issue of spatial and frequency diversity, the model here makes several simplifying assumptions. Each platform uses an N-element, side-mounted, uniformly spaced, linear array and M coherent narrowband pulses within a single CPI. All platforms are assumed to use the same pulse repetition interval (PRI) T.

A. Target Model

The signal components in (2) and (4), for a chosen look point and look velocity and transmission from platform q received at platform p, are defined in terms of target amplitude α_{pq} and the target space-time steering vector $\mathbf{g}_{pq}$. The definition of this steering vector is fundamental to both the data model and the adaptive processing schemes used. It is assumed here that the target exhibits coherent scattering over the bandwidth of individual transmissions.

The target steering vector $\mathbf{g}_{pq}$ is a function of the look point and look velocity in relation to the locations and velocities of platforms p and q:

$$
\mathbf{g}_{pq} = \mathbf{t}_{pq} \otimes \mathbf{s}_{pq} \qquad (6)
$$

where $\mathbf{t}_{pq}$ and $\mathbf{s}_{pq}$ are, respectively, the temporal and spatial components of the target space-time steering vector and $\otimes$ denotes the Kronecker product.

[2]We are inherently assuming that the center frequencies are spaced far enough apart to eliminate cross-correlations between different frequencies.

The temporal steering vector is the length-M vector received at the platform due to a unit amplitude target moving with the look velocity. Then, the temporal steering vector, for a slowly fluctuating target, at platform p due to the signal from platform q is

$$\mathbf{t}_{pq} = [1, \exp(j2\pi\varpi^t_{pq}), \exp(j2\pi\varpi^t_{pq}2), \ldots, \exp(j2\pi\varpi^t_{pq}(M-1))]^T \tag{7}$$

where $\varpi^t_{pq} = f^t_{pq}T$ is the Doppler frequency f^t_{pq} normalized with the common PRI T.

For simplicity, to obtain the spatial component in (6), we ignore any crab angle. The spatial steering vector for platform p for the transmission from platform q is then given by

$$\mathbf{s}_{pq} = [1, \exp(j2\pi\varpi^s_{pq}), \exp(j2\pi\varpi^s_{pq}2), \ldots, \exp(j2\pi\varpi^s_{pq}(N-1))]^T \tag{8}$$

where $\varpi^s_{pq} = d\bar{a}_p \cdot \bar{r}^t_p/\lambda_q$ is the normalized spatial frequency of the target, d is the interelement spacing, λ_q is the wavelength corresponding to frequency f_q, $\bar{a}_p$ and $\bar{r}^t_p$ are the unit vector along the antenna array at platform p and the unit vector pointing from platform q to the target, respectively.

Note that without frequency diversity (the NFD case) the spatial steering vector, for platform p, is common to all K transmissions, i.e., the K transmissions cannot be distinguished. As we will see, this implies that fully $K-1$ of the transmissions then act as interference and hinder the detection process.

B. Interference Model

In this section we develop the model for the EMI and clutter interference components individually. The approach taken is similar to that for a monostatic airborne radar [12].

1) *Electromagnetic Interference*: The received signal due to EMI in the distributed configuration is basically same as in the monostatic case; it has the characteristics of a point target in the spatial domain, but of thermal noise in the temporal domain.

If there exist N_j EMI sources, the overall space-time snapshot of the EMI signal at platform p can be expressed as follows

$$\mathbf{j} = \sum_{l=1}^{N_j} \boldsymbol{\alpha}^j_l \otimes \mathbf{s}^j_l \tag{9}$$

where $\boldsymbol{\alpha}^j_l = [\alpha^j_{l0}, \alpha^j_{l1}, \ldots, \alpha^j_{l(M-1)}]^T$ is a complex Gaussian random vector with $\mathrm{E}\{\boldsymbol{\alpha}^j_l \boldsymbol{\alpha}^{j^H}_l\} = \sigma^2_l \mathbf{I}_M$, where σ^2_l represents the power of the lth source. The spatial steering vector of lth interfering signal $\mathbf{s}^j_l$ can be defined similar to (8).

2) *Clutter*: To model the clutter, a distributed RF sensor system can be considered as a generalization of a bistatic system. The signal received at a platform is due the signal transmitted by itself (in a monostatic configuration) and due the other $K-1$ platforms, each of which are in bistatic configurations. Furthermore, since a monostatic system is a special case of bistatic radar we focus on bistatic radar systems [17] exclusively.

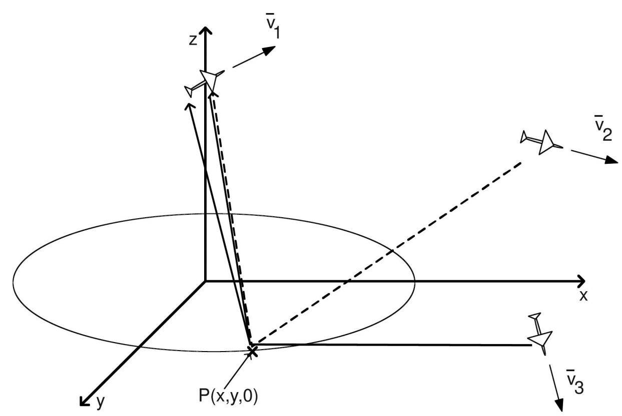

Fig. 2. Geometry for multistatic system.

As in [12] the clutter signal is modeled here as the sum over the contributions over many small clutter patches. Each individual patch can be described in a manner similar to the target signal. This paper assumes there are no ambiguous ranges which may be treated by repeated implementation of the model presented here. The clutter signal received at platform p is the superposition of the signals from all clutter patches at the iso-range associated with the target range.

Assuming a flat Earth, the iso-range contours of a bistatic radar system, are the intersection of the ellipsoid of revolution, with foci at the transmit and receive sites, with the ground plane. However, from the point of view of a receiving platform the iso-range is the same as that of a monostatic radar. This becomes relevant when determining the training data to be used in a STAP implementation. Fig. 2 illustrates this concept, though not shown in the figure is the shift in this iso-range contour due to the true time delay, as described in Section II, on transmit and receive.

The clutter signal received at antenna l of platform p due to the PRI m from the signal transmitted by platform q is

$$c^{lm}_{pq} = V_0 \sum_{r=1}^{N_c} a_{cr} G_{lr} \exp(j2\pi f^{cr}_{pq} mT) \exp\left(j\frac{2\pi}{\lambda_q}\bar{y}^l_p \cdot \bar{r}^r_p\right) \exp(j\varphi_{pqr}) \tag{10}$$

where N_c is the total number of clutter patches in the iso-range, a_{cr} is random complex amplitude of rth clutter patch, G_{lr} is the gain factor of antenna l toward the rth clutter patch, V_0 is amplitude of the transmit signal, and $\bar{r}^r_p$ is a unit vector from platform p to rth clutter patch. $\varphi_{pqr} = -2\pi R_{pqr}/\lambda_q$ is a phase constant where R_{pqr} is the total distance from platform q clutter

TABLE I
Common Parameters

Parameter	Value
System Parameters	
Frequency Offset	20 MHz
Interelement Spacing	0.1 m
Peak Transmit Power	200 KW
Instantaneous BW	4 MHz
System Loss	4 dB
PRF	1 KHz
M	10
N	10
K	3
Clutter Parameters	
Ground Reflectivity	−3 dB
Number of Clutter Patches	360
Clutter to Noise Ratio	70 dB

TABLE II
Platform Parameters

Parameter	Value
Platform 1	
Operating Frequency(NFD & FD)	450 MHz
Location	$(0,0,3\times10^3)$
Velocity	100 m/s
Moving Direction	$(0,1,0)$
$\bar{a}_1$	$(0,1,0)$
Platform 2	
Operating Frequency (NFD)	450 MHz
Operating Frequency (FD)	430 MHz
Location	$(20\times10^3,16\times10^3,3\times10^3)$
Velocity	100 m/s
Moving Direction	$(1,0,0)$
$\bar{a}_2$	$(1,0,0)$
Platform 3	
Operating Frequency (NFD)	450 MHz
Operating Frequency (FD)	410 MHz
Location	$(20\times10^3,-24\times10^3,3\times10^3)$
Velocity	100 m/s
Moving Direction	$(-1,0,0)$
$\bar{a}_3$	$(-1,0,0)$

patch r and then to platform p. f_{pq}^{cr} is the Doppler frequency of the rth clutter patch.

The gain factor G_{lr} in (10) is defined as

$$G_{lr} = \begin{cases} \dfrac{\lambda_q F_T(\bar{r}_q^r)F_{Rl}(\bar{r}_p^r)\sqrt{\sigma_r^0 \Delta A_r P_t}}{\sqrt{(4\pi)^3 L_s N_0} R_{pr} R_{qr}} & \\ & \text{for} \quad R_{pr} < R_{R\max} \\ & \text{and } R_{qr} < R_{T\max}, \\ 0, & \text{elsewhere} \end{cases} \tag{11}$$

where $F_T(\bar{r}_q^r)$ is the transmit voltage pattern in the direction of $\bar{r}_r^q$, $F_{Rl}(\bar{r}_p^r)$ is the antenna field gain of receive channel l in direction $\bar{r}_p^r$, σ_r^0 is the ground reflectivity of the rth clutter patch of area ΔA_r, P_t is the peak transmit power, L_s is the system loss, N_0 is the receiver noise power spectral density, and R_{qr} is the distance between platform q and clutter patch r. The maximum receive and transmit distances $R_{R\max} = 130\sqrt{h_p}$ and $R_{T\max} = 130\sqrt{h_q}$ are the range-to-horizon of the receiver and transmitter platform, respectively, in kilometers where $h_q, q = 1,2,\ldots,K$ is the height of platform q [17]. The clutter area of the rth patch ΔA_r can be approximated as [19]

$$\Delta A_r \approx \frac{c\tau R_{pr}\Delta\theta_r}{2\cos^2(\beta_r/2)} \tag{12}$$

where τ is the pulse width, $\Delta\theta_r$ is the azimuth angular extent of the rth clutter patch seen by the receiver, and β_r is the angle between the transmitter and the receiver seen by the rth clutter patch.

Therefore, using the space-time steering vector $\mathbf{g}_{pq}^{cr}$ of the rth clutter patch the overall clutter space-time snapshot created at platform p by the signal transmitted by platform q for one iso-range contour is

$$\mathbf{c}_{pq} = V_0 \sum_{r=1}^{N_c} a_{cr}\mathbf{G}_r \odot \mathbf{g}_{pq}^{cr} \exp(j\varphi_{pqr}) \tag{13}$$

where $\odot$ represents the Hadamard (element-wise) product, a_{cr} is a complex random amplitude and $\mathbf{G}_r = \mathbf{1}_M \otimes [G_{0r}, G_{1r}, \ldots, G_{(N-1)r}]^T$ is the channel gain vector. Here $\mathbf{1}_M$ is a length-M column vector of ones. The amplitude a_{cr} is modeled as a zero-mean, complex Gaussian random variable $\mathcal{CN}(0,\sigma_{cr}^2)$ with variance σ_{cr}^2 determined by the chosen total clutter power. The variance is weighted by transmit and receive beampatterns.

IV. PERFORMANCE METRICS: SINR AND PROBABILITY OF DETECTION

This section presents the results of simulations illustrating the performance of the two systems (NFD and FD) considered. This performance is measured using two figures of merit: the output SINR after adaptive processing and probability of detection for a given probability of false alarm. Unless stated otherwise, the parameters used in the simulations are given in Tables I and II.

A. Signal-to-Interference-plus-Noise Ratio

Using STAP the NM signals at the pth platform in the distributed system are multiplied with a weight vector $\mathbf{w}_p = \mathbf{R}_p^{-1}\mathbf{g}_p$, $p = 1,\ldots,K$. The overall SINR of the K-platform multistatic radar system, defined as the ratio of powers of the output signal component to the interference plus noise component is given by

$$\text{SINR} = \frac{\sum_{p=1}^K \delta^2 \xi_{tp} |\mathbf{w}_p^H \mathbf{g}_p|^2}{\sum_{p=1}^K \mathbf{w}_p^H \mathbf{R}_p \mathbf{w}_p} \tag{14}$$

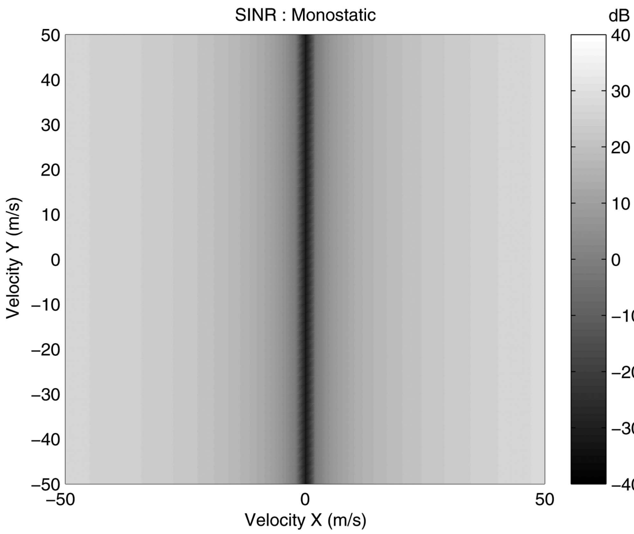

Fig. 3. SINR at platform 1: Monostatic case.

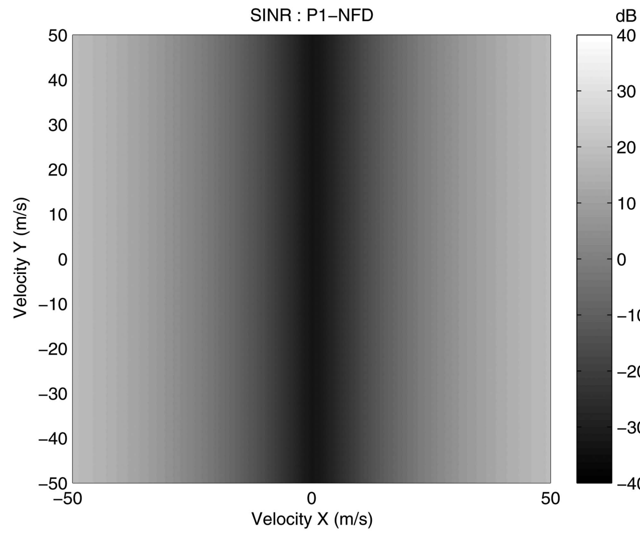

Fig. 4. SINR at platform 1: P1-NFD case.

where δ^2 is the noise power per element, ξ_{tp} is the target signal-to-noise ratio (SNR) on a single pulse and array element at platform p, $\mathbf{w}_p$, $\mathbf{g}_p$ and $\mathbf{R}_p$ are the weight vector, target space-time steering vector, and covariance matrix of the unwanted signals at platform p, respectively. Unless stated otherwise, the simulations assume each platform has the same SNR.

The first simulation illustrates the drawbacks of relying on a monostatic system, corresponding to using only platform 1 from Table II. Fig. 3 plots the SINR of this monostatic system, as a function of look velocities in the x and y directions. The target is located at $(20 \times 10^3, 0, 0)$ with SNR of 0 dB. As is clear from the figure, since the platform is moving along the y-axis, the SINR of monostatic radar is independent of the y-component of the look velocity. The loss in SINR at the clutter ridge (x-component of the velocity is 0) is also clear. As expected, a monostatic system is unable to detect targets with low radial, though potentially high absolute, speed.

Figs. 4 and 5 plot the SINR of platform 1 in NFD and FD cases, respectively. These figures illustrate the benefits of frequency diversity. In the NFD case, because each platform sees the multiple transmissions as interference, the SINR plot is worse than the monostatic case; the loss in SINR near the clutter ridge is wider. On the other hand, because each transmission can be independently exploited, the FD case clearly shows an enhanced SINR result than the NFD case and monostatic cases. As illustrated in Fig. 3 previously, the SINR deduction, associated with platform 1, is maximum along the y-axis. In the FD case, for higher y-components of target velocity, the other platforms contribute significant signal components

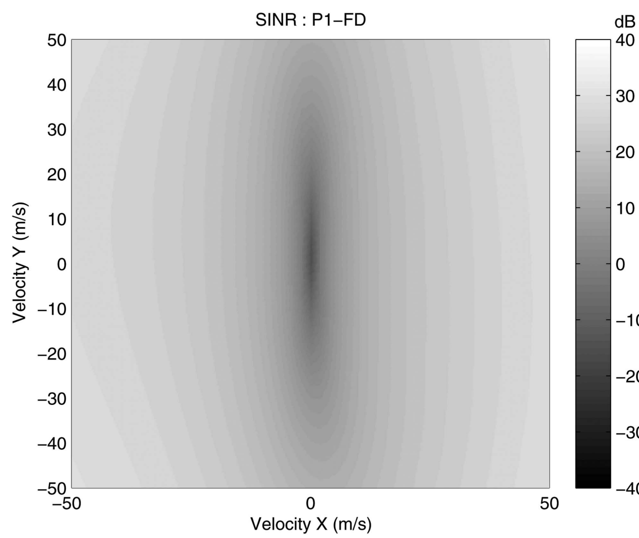

Fig. 5. SINR at platform 1: P1-FD case.

in a bistatic mode, in turn resulting in higher SINR. This is in contrast to the NFD case where the multiple transmissions mutually interfere, resulting in a wide SINR notch.

Figs. 6 and 7 plot the overall SINR of the NFD case and FD cases, respectively. Compared with the single platform results in Figs. 4 and 5, the overall response illustrates the benefits of spatial diversity. Since the directions of platforms 2 and 3 are perpendicular to that of platform 1, the corresponding SINR notches are not aligned. In addition to the velocities of the platforms, the geometry of platforms plays an important role in multistatic radar. Different geometries result in different Doppler frequencies even though velocities of platforms are the same. This is the main advantage of multistatic radar. By viewing the target from different aspect angles, these two figures show that the SINR can be improved. The overall response has a null only in the low

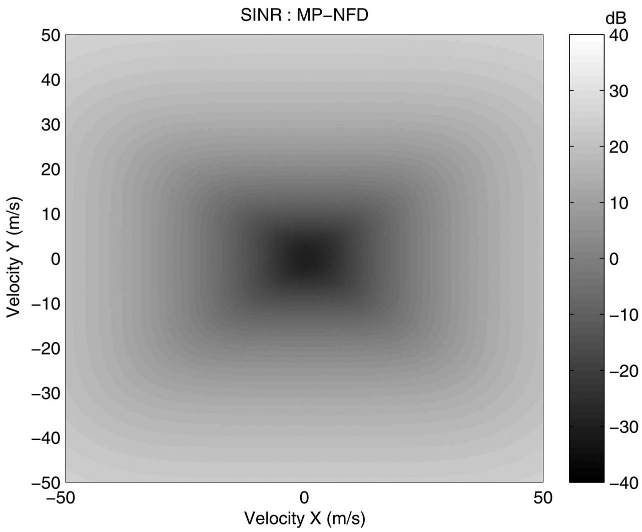

Fig. 6. SINR using multiple platforms: MP-NFD case.

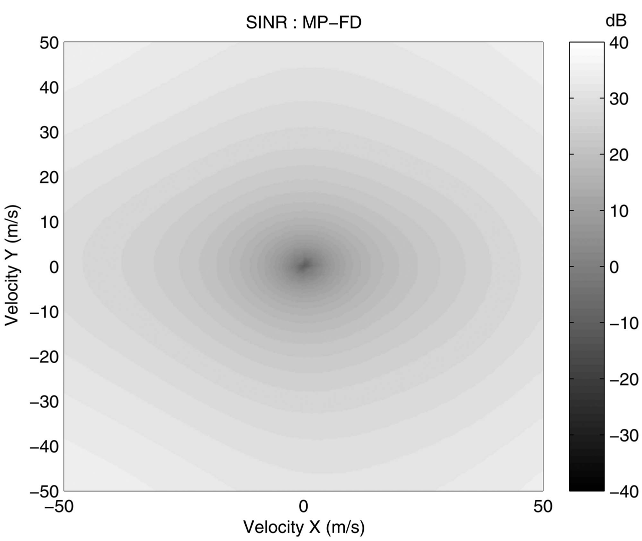

Fig. 7. SINR using multiple platforms: MP-FD case.

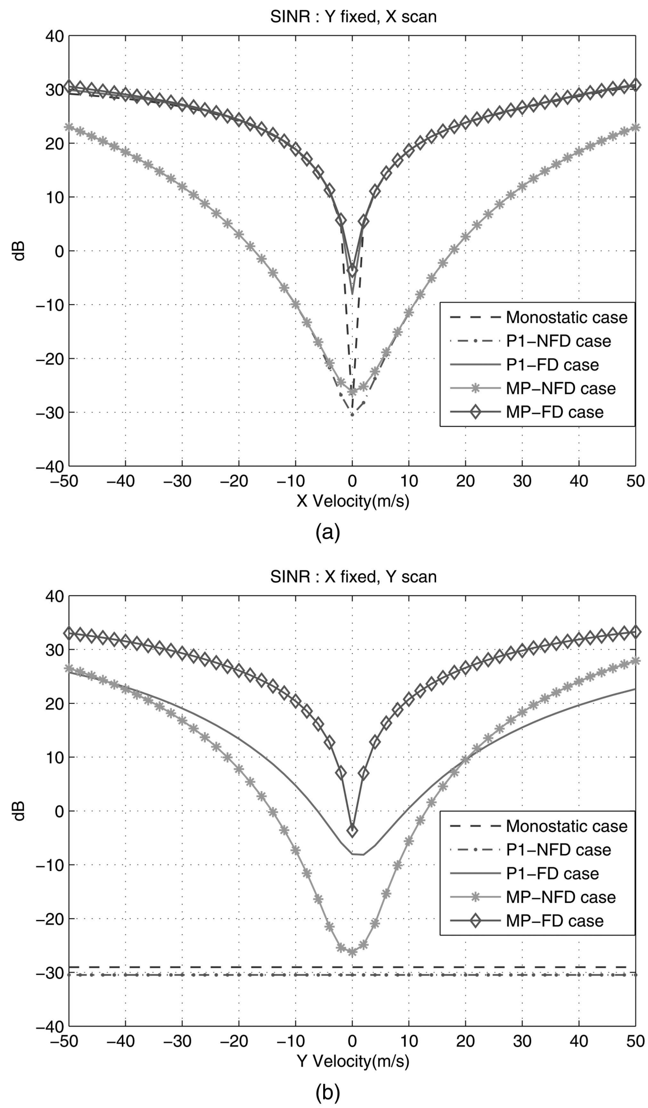

Fig. 8. SINR plots along specific x- and y-target velocity components. (a) Cut along Y-axis, $v_y = 0$ m/s. (b) Cut along X-axis, $v_x = 0$ m/s.

absolute-velocity region which is around the clutter ridge regardless of target direction. Note that this spatial diversity can be obtained in both the NFD and FD case. However, clearly, the combination of frequency and spatial diversity in the FD case leads to significantly improved performance over the NFD case.

It is worth comparing these results with that in [15]; there the authors assumed that each platform receives a signal from itself only, i.e., that each platform receives data in a monostatic configuration only. The underlying assumption is that orthogonal signals are used. However, this paper shows SINR enhancement by using not only monostatic reflection but also bistatic reflections. This leads to higher detection probability which is shown in the following section.

Fig. 8 plots one-dimensional cuts of all these figures along the zero x- and y-target velocity components. The multiple platform, frequency diverse (MP-FD) curve clearly indicates the best performance among all schemes. Note that the case without frequency diversity (MP-NFD) shows marked improvement over the single-platform NFD case, i.e., spatial diversity provides robustness as expected. However, the performance is still significantly worse than the case with frequency diversity. Taken together, a significant improvement when using spatial diversity in conjunction with frequency diversity is achieved, i.e., the advantages of the scheme proposed and developed in this paper are clear. These gains of the MP-FD scheme also translate to the minimum detectable velocity (MDV). The width of the SINR notch of the MP-NF cases for zero x- and y-target velocity, at 0 dB SINR, are 35 m/s, 26 m/s, respectively. The corresponding numbers are 1.5 m/s and 1.25 m/s for the MP-FD case.

B. Probability of Detection

In distributed radar networks, a popular approach is based upon purely distributed detection which uses an independent target-detection test at each platform and then merges these binary decisions at a centralized processor (e.g., using the OR rule) [1, 20]. Each platform may use an optimized threshold to maximize the detection probability P_D while maintaining a fixed false alarm rate P_{FA}. This distributed approach is clearly suboptimal and improved detection performance could be achieved if all platforms signals were processed jointly. While joint processing would place an enormous burden on required inter-platform communication and computation load, joint processing also provides an upper bound on the system performance.

The test statistic of the optimum centralized detector is defined as [15]

$$\begin{aligned} \text{NFD case}: \quad z &= \sum_{p=1}^{K} \frac{|\mathbf{w}_p^H \mathbf{x}_p|^2}{1/\sigma_{tp}^2 + \mathbf{g}_p^H \mathbf{R}_p^{-1} \mathbf{g}_p} \\ \text{FD case}: \quad z &= \sum_{p=1}^{K}\sum_{q=1}^{K} \frac{|\mathbf{w}_{pq}^H \mathbf{x}_q|^2}{1/\sigma_{tpq}^2 + \mathbf{g}_{pq}^H \mathbf{R}_{pq}^{-1} \mathbf{g}_{pq}} \end{aligned} \tag{15}$$

where the adaptive weights are given by $\mathbf{w}_p = \mathbf{R}_{up}^{-1}\mathbf{g}_p$ for the NFD case and $\mathbf{w}_{pq} = \mathbf{R}_{pq}^{-1}\mathbf{g}_{pq}$ for the FD case. For notational convenience, if we rearrange the indices such that $j = p$ for the NFD case and $j = K(p-1) + q$ for the FD case, (15) can be unified as follows

$$z = \sum_{j=1}^{J} \frac{|\mathbf{w}_j^H \mathbf{x}_j|^2}{1/\sigma_{tj}^2 + \mathbf{g}_j^H \mathbf{R}_j^{-1} \mathbf{g}_j} \tag{16}$$

where $J = K$ and K^2 for the NFD and FD cases, respectively.

Using this statistic, the probability of detection (P_D), as derived in the Appendix, is

$$P_D = \sum_{j=1}^{J} \left(\prod_{l=1,\ l\neq j}^{J} (A_{1j} - A_{1l})^{-1} \right) A_{1j}^{J-1} e^{-\Lambda/A_{1j}} \tag{17}$$

where $A_{1j} = \lambda_{0j}(1 + \lambda_{0j}\sigma_{tj}^2)/\alpha_j$ and $\lambda_{0j} = \mathbf{g}_j^H \mathbf{R}_j^{-1} \mathbf{g}_j$.

Fig. 9 plots the probability of detection seen by platform 1 with common probability of false alarm $P_{FA} = 10^{-6}$ and SNR = 15 dB. The parameters used in these simulations are given in Tables I and II. The target speed is fixed to 10 m/s and the target is located at $(20 \times 10^3, 0, 0)$. The direction of the target is measured counterclockwise from the positive x-axis. `Pp-NFD` and `Pp-FD` represent the detection probability of the NFD and FD cases at the pth platform, respectively. `Ppq` is the P_D of the (monostatic or bistatic) scenario with signal transmitted from platform q and received at platform p. Finally, the plot also includes the OR case (where a target is declared present if any of platforms identifies a target). `Pp-FD-OR` is the P_D when using the OR processor combining P_D of each incoming signal as follows

$$\texttt{P1-FD-OR} = 1 - (1 - \texttt{P11})(1 - \texttt{P12})(1 - \texttt{P13}) \tag{18}$$

since the events corresponding to `P11`, `P12`, and `P13` are independent.

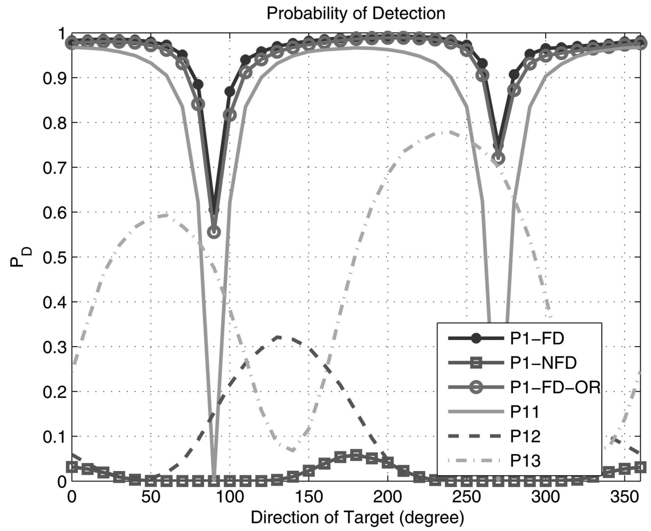

Fig. 9. Probability of detection with $P_{FA} = 10^{-6}$, SNR = 15 dB.

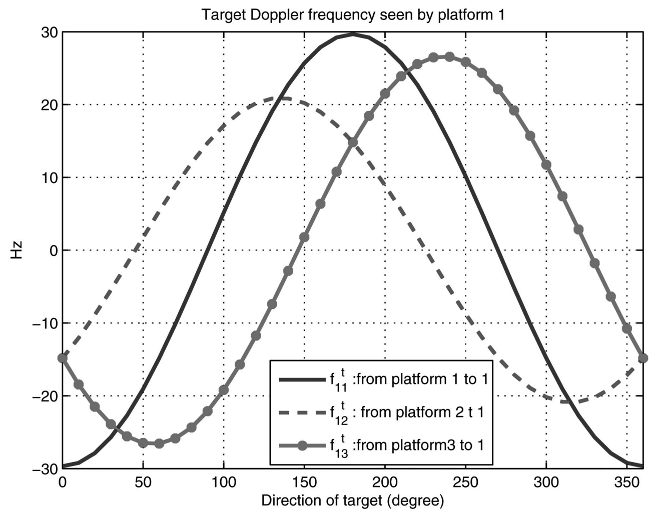

Fig. 10. Target Doppler frequency seen by platform 1.

As can be seen in the figure, the FD case (`P1-FD`) has the highest P_D among all cases. From the figure, the impact of varying the Doppler frequency on the monostatic configuration is clear; the P_D of the monostatic configuration (`P11`) varies significantly more than that of bistatic configuration (`P12` and `P13`). Even though the target speed remains constant, the Doppler frequency depends on the relative motion of the target and platform. On the other hand, in a bistatic configuration, the Doppler frequency is a function of both the transmitter and receiver velocities resulting in an inherent robustness.

This discussion related to Fig. 9 is reinforced by the results in Fig. 10. Each of the `P11`, `P12`,

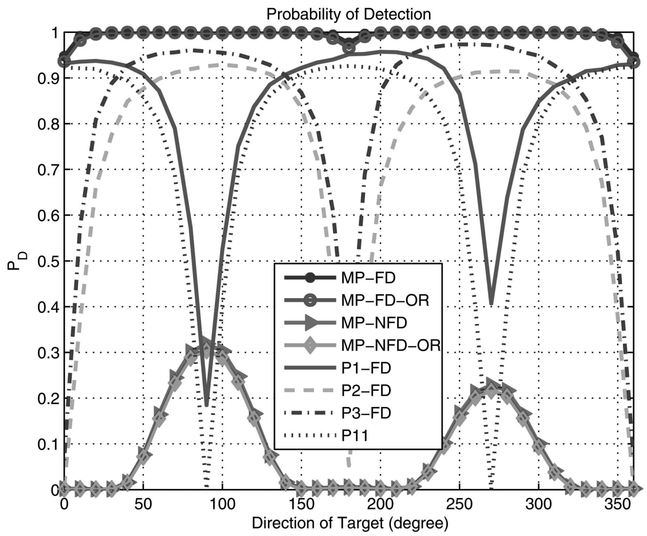

Fig. 11. Probability of detection with $P_{\mathrm{FA}} = 10^{-6}$, SNR = 10 dB.

and `P13` cases has low P_{D} when it falls in the low Doppler frequency region around 0 Hz and the P_{D} becomes larger as the absolute value of the Doppler frequency becomes higher. When the target moves along the positive y-axis (90° in Figs. 9 and 10), Platform 1 cannot detect the target using only the monostatic configuration (`P11`) since the Doppler frequency is zero. This is consistent with the SINR result in Fig. 3. However, bistatic configurations `P12` and `P13` contribute to the `P1-FD` within platform 1. We also can see that monostatic configuration still has a dominant effect on `P1-FD` except for the low velocity region. In the FD case, the bistatic Doppler frequencies are never all zero, i.e., nulls of the P_{D} in a bistatic configuration do not coincide with those in a monostatic configuration. This is the main advantage of using frequency diversity. As earlier, the NFD case (`P1-NFD`) results in extremely poor performance because signals from other platforms act as EMI.

Fig. 11 plots the probability of detection P_{D} of the overall multistatic system with target SNR = 10 dB. In this example, the false alarm rate is again $P_{\mathrm{FA}} = 10^{-6}$ and the target velocity is 10 m/s. `MP-NFD` and `MP-FD` are, respectively, the P_{D} of the optimum multi-platform NFD and FD cases using (17). `MP-NFD-OR` and `MP-FD-OR` represent the P_{D} of the output of the OR processor for the NFD and FD cases, respectively, based on the binary decision at each platform. Note that since the data is independent from each platform, the output of the OR processor can be analyzed in a manner similar to (18).

Fig. 11 illustrates the gains due to spatial and frequency diversity in a distributed aperture system. In both NFD and FD cases, the overall P_{D} has significantly less fluctuation than the P_{D} from the other cases. This is because the relative motions and aspect angles to each platform are different. Minima (and maxima) in the P_{D} curves for each platform arise

TABLE III
Target Parameters

Parameter	Value
Location	$(20 \times 10^3, 0, 0)$
Speed	10 m/s
Moving Direction	$(1, 3, 0)/\sqrt{10}$

at different target velocities and angles; combining the data from multiple platforms in an optimal way, therefore, results in a "uniform" P_{D} curve regardless of target direction.

These results are a direct result of the geometry and velocity directions given in Table II. Platform 2 and 3 are moving perpendicular to the platform 1. Because of the geometry and moving directions, nulls in P_{D} of Platform 2 and 3 (`P2-FD` and `P3-FD`) do not coincide with the null in P_{D} of platform 1 (`P1-FD`) and the overall P_{D} shows robustness to the target direction. As a result, the overall P_{D} is almost uniform as compared with `P1-FD`, `P2-FD`, or `P3-FD`. In addition, frequency diversity enhances performance. The FD case has a higher P_{D} than the NFD case in both Fig. 9 and Fig. 11. As mentioned several times now, this is due to the fact that the NFD case must treat signals from other platforms as interference.

For completeness, Figs. 12 and 13 plot the more traditional P_{D} versus SNR curves for the cases considered above. Given the target parameters in Table III, Figs. 12 and 13 are the P_{D} seen by platform 1 and the overall P_{D}, respectively. Fig. 12 illustrate the advantage of the FD case over the NFD case for the single platform case seen by platform 1. In addition, the P_{D} of the OR processor (`P1-FD-OR`) is very close to P_{D} seen by platform 1 in the FD case (`P1-FD`). Fig. 13 plots the overall P_{D}. As with the single platform case, using frequency diversity provides for a higher detection probability. Again, the OR processor, `MP-FD-OR` and `MP-NFD-OR` performs very close to the optimal case `MP-FD` and `MP-NFD`, respectively.

One should emphasize that the OR processors in the single and distributed platform cases are similar theoretically, but significantly different conceptually. In the single platform case, since the data is gathered within the same platform, communication bandwidth is not an important issue. However, when all platforms work together to decide on a hypothesis, communication bandwidth plays an important role since the data collected at each platform has to be transferred to a fusion center [20]. Since each transmission can be isolated, the FD requires a K-fold increase in communication bandwidth. Using Fig. 13, a strong argument could be made for the OR processor, wherein only binary decisions are communicated, across platforms.

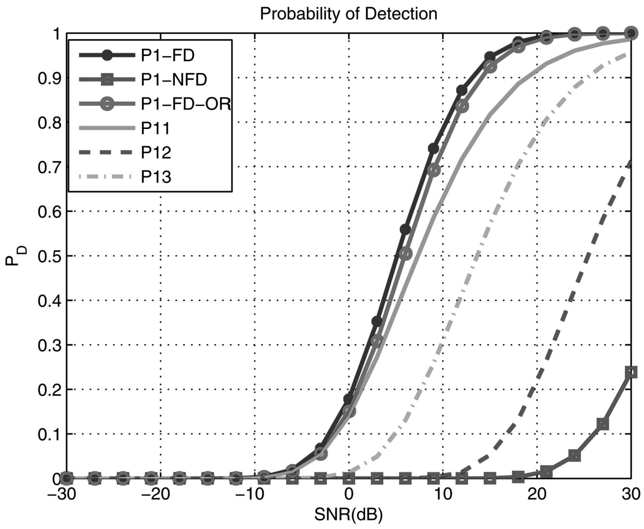

Fig. 12. Probability of detection with $P_{\mathrm{FA}} = 10^{-6}$.

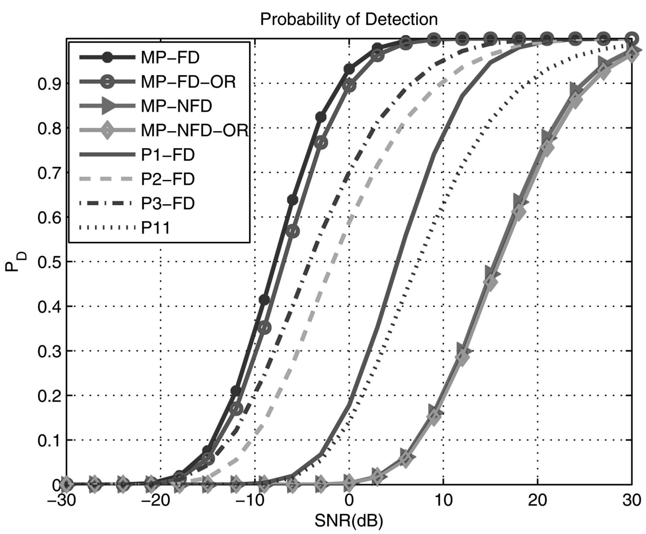

Fig. 13. Probability of detection with $P_{\mathrm{FA}} = 10^{-6}$.

V. CONCLUSION

This paper developed and analyzed the case of detection over a distributed array of sensors. Of crucial importance is the use of true time delay such that the transmitted signals arrive at the look point simultaneously, i.e., a single time sample corresponds to the look point. In this paper we developed a data model for the two cases when frequency diversity is (the FD case) and is not used (the NFD case). The use of frequency diversity is shown to be important because, in the NFD case, transmissions from multiple platforms interfere with each other and increase, rather than decrease, the overall interference level.

The system and data models developed in Sections II and III, respectively, provide the basis for the analysis that follows. The analysis investigated the output SINR and probability of detection. As is clear from the results, the benefits of using frequency and spatial diversity are significant. Previous work has largely focused on spatial diversity exclusively. However, by not considering frequency diversity, signals from other platforms contribute to undesired interference at each platform, significantly worsening performance possibly below even the single platform case. Frequency diversity allows for the discrimination of signals from different platforms and alleviates this situation.

One drawback of the frequency diversity scheme presented here is that each platform must possess K entire receive processing chains. This concern may be addressed by the use of orthogonal frequency division multiplexing (OFDM) [18]. However, OFDM itself has its own drawbacks that must be addressed in any implementation. Another potential avenue for research is the use of orthogonal code division multiple access to isolate individual transmissions. A final issue not considered here is the implementation of the STAP algorithm. Even though STAP is optimum in the sense of maximizing SINR and P_{D} for a given P_{FA}, it is almost impossible to implement in practice due to the associated computation load and, fundamentally, the required sample support [12, 21]. The problem becomes even worse when applied to a distributed sensor system. The issue of sample support arises because the interference covariance matrix must be estimated using training data. Reduced rank STAP algorithms for distributed sensor systems are an open research topic.

APPENDIX. PROOF OF THE PROBABILITY OF DETECTION

In this Appendix we derive the probability of detection P_{D} and probability of false alarm P_{FA} for the cases of distributed and joint processing of the signals.

In (16) define $\alpha_j = 1/\sigma_{tj}^2 + \mathbf{g}_j^H \mathbf{R}_j^{-1}\mathbf{g}_j$, $y_j = \mathbf{w}_j^H \mathbf{x}_j$ and $z_j = |y_j|^2 = |\mathbf{w}_j^H \mathbf{x}_j|^2$, then it can be simplified as

$$z = \sum_{j=1}^{J} \frac{1}{\alpha_j} z_j. \tag{19}$$

Since $y_j \sim \mathcal{CN}(0, \sigma_{yj}^2)$, its variance σ_{yj}^2 is given as

$$\begin{aligned}\boldsymbol{\sigma}_{yj}^2 &= \mathrm{E}\{y_j y_j^*\} = \mathrm{E}\{\mathbf{w}_j^H \mathbf{x}_j \mathbf{x}_j^H \mathbf{w}_j\} = \mathbf{w}_j^H \mathrm{E}\{\mathbf{x}_j \mathbf{x}_j^H\}\mathbf{w}_j \\ &= \mathbf{w}_j^H \mathbf{R}_j \mathbf{w}_j = \mathbf{g}_j^H \mathbf{R}_j^{-1} \mathbf{R}_{xj} \mathbf{R}_j^{-1} \mathbf{g}_j\end{aligned} \tag{20}$$

where $\mathbf{R}_{xj} = E[\mathbf{x}_j \mathbf{x}_j^H]$ is the covariance matrix of the received signal depending on each hypotheses as follows

$$\begin{aligned} H_0: &\quad \mathbf{R}_{xj} = \mathbf{R}_j \\ H_1: &\quad \mathbf{R}_{xj} = \mathbf{R}_j + \mathbf{R}_{sj}. \end{aligned} \tag{21}$$

Given these developments, the random variable z_j is exponential with mean σ_{yj}^2, i.e., its probability density function (pdf) is

$$f_{Z_j}(z_j) = \frac{1}{\sigma_{yj}^2} e^{-z_j/\sigma_{yj}^2}. \tag{22}$$

For the target-absent (H_0) and target-present (H_1) hypotheses, (20) results in

$$\begin{aligned}\sigma_{yj}^2 \mid H_0 &= \mathbf{g}_j^H \mathbf{R}_j^{-1} \mathbf{R}_{xj} \mathbf{R}_j^{-1} \mathbf{g}_j \\ &= \mathbf{g}_j^H \mathbf{R}_j^{-1} \mathbf{g}_j, \\ \sigma_{yj}^2 \mid H_1 &= \mathbf{g}_j^H \mathbf{R}_j^{-1} (\mathbf{R}_{sj} + \mathbf{R}_j) \mathbf{R}_j^{-1} \mathbf{g}_j \\ &= \mathbf{g}_j^H \mathbf{R}_j^{-1} \mathbf{R}_{sj} \mathbf{R}_j^{-1} \mathbf{g}_j + \mathbf{g}_j^H \mathbf{R}_j^{-1} \mathbf{g}_j \qquad (23)\end{aligned}$$

where $\mathbf{R}_{sj} = \sigma_{tj}^2 \mathbf{g}_j \mathbf{g}_j^H$.

Let $\bar{z}_j$, $j = 1, 2, \ldots, J$ be independent and identically distributed (IID) standard exponential random variables and define $\lambda_{0j} = \mathbf{g}_j^H \mathbf{R}_j^{-1} \mathbf{g}_j$. Then (19) can be rewritten as

$$z = \sum_{j=1}^{J} \frac{\sigma_{yj}^2 \mid H_0}{\alpha_j} \bar{z}_j = \sum_{j=1}^{J} \frac{\lambda_{0j}}{\alpha_j} \bar{z}_j. \qquad (24)$$

Since z is the weighted sum of standard exponential random variables, its pdf is [22]

$$f_Z(z) = \sum_{j=1}^{J} \left(\prod_{l=1,\ l \neq j}^{J} (A_{0j} - A_{0l})^{-1} \right) A_{0j}^{J-2} e^{-z/A_{0j}} \qquad (25)$$

where $A_{0j} = \lambda_{0j}/\alpha_j$.

The false alarm rate (P_{FA}) corresponding to a threshold Λ is, therefore, given by

$$\begin{aligned}P_{\text{FA}} &= \int_{\Lambda}^{\infty} \sum_{j=1}^{J} \left(\prod_{l=1,\ l \neq j}^{J} (A_{0j} - A_{0l})^{-1} \right) A_{0j}^{J-2} e^{-z/A_{0j}} dz \\ &= \sum_{j=1}^{J} \left(\prod_{l=1,\ l \neq j}^{J} (A_{0j} - A_{0l})^{-1} \right) A_{0j}^{J-1} e^{-\Lambda/A_{0j}}. \qquad (26)\end{aligned}$$

The required threshold for a given P_{FA} can therefore be found via a one-dimensional search to invert (26).

The probability of detection (P_{D}) can be obtained in the similar manner, resulting in

$$P_{\text{D}} = \sum_{j=1}^{J} \left(\prod_{l=1,\ l \neq j}^{J} (A_{1j} - A_{1l})^{-1} \right) A_{1j}^{J-1} e^{-\Lambda/A_{1j}} \qquad (27)$$

where $A_{1j} = \lambda_{0j}(1 + \lambda_{0j}\sigma_{tj}^2)/\alpha_j$.

REFERENCES

[1] Chernyak, V. S.
Fundamentals of Multisite Radar Systems: Multistatic Radars and Multiradar Systems, (1st ed.).
London: CRC Press, 1998.

[2] Hanle, E.
Survey of bistatic and multistatic radar.
IEE Proceedings, **133**, 7 (Dec. 1986), 587–595.

[3] Conte, E., et al.
Multistatic radar detection: Synthesis and comparison of optimum and suboptimum receivers.
IEE Proceedings, **130**, 6 (Oct. 1983), 484–494.

[4] D'Addio, E. and Farina, A.
Overview of detection theory in multistatic radar.
IEE Proceedings, **133**, 7 (Dec. 1986), 587–595.

[5] Mrstik, A.
Multistatic-radar binomial detection.
IEEE Transactions on Aerospace and Electronic Systems, **AES-14**, 1 (Jan. 1978), 103–108.

[6] Bradaric, I., et al.
Multistatic radar systems signal processing.
In *Proceedings of the IEEE Radar Conference*, Apr. 2006, 106–113.

[7] Fishler, E., et al.
Spatial diversity in radars—Models and detection performance.
IEEE Transactions on Signal Processing, **54**, 3 (Mar. 2006), 823–838.

[8] Bruyere, D. and Goodman, N.
Performance of multistatic space-time adaptive processing.
In *Proceedings of the IEEE Radar Conference*, Apr. 2006, 533–538.

[9] Adve, R., et al.
Space-time adaptive processing for distributed aperture radars.
Presented at the 1st IEE Waveform Diversity Conference, Nov. 2004.

[10] Abramovich, Y. and Frazer, G.
Bounds on the volume and height distributions for the MIMO radar ambiguity function.
IEEE Signal Processing Letters, **15** (2008), 505–508.

[11] Klemm, R.
Principles of Space-Time Adaptive Processing (2nd ed.).
London: IEE Press, 2002.

[12] Ward, J.
Space-time adaptive processing for airborne radar.
MIT Lincoln Laboratory, Cambridge, MA, 1994.

[13] Melvin, W., Callahan, M., and Wicks, M.
Bistatic STAP: Application to airborne radar.
In *Proceedings of the IEEE Radar Conference*, Apr. 2002, 1–7.

[14] Himed, B., Michels, J., and Zhang, Y.
Bistatic STAP performance analysis in radar applications.
In *Proceedings of the IEEE Radar Conference*, Apr. 2001, 60–65.

[15] Goodman, N. and Bruyere, D.
Optimum and decentralized detection for multistatic airborne radar.
IEEE Transactions on Aerospace and Electronic Systems, **43**, 2 (Apr. 2007), 806–813.

[16] Jackson, M.
The geometry of bistatic radar systems.
IEE Proceedings, **133**, 7 (Dec. 1986), 604–612.

[17] Zhang, Y.
Bistatic space-time adaptive processing (STAP) for airborne/spaceborne application.
Air Force Research Laboratory, Technical Report F30602-98-C-0125, 1999, Final report by Stiefvater Consultants.

[18] Lock, E. and Adve, R.
Orthogonal frequency division multiplexing in distributed radar apertures.
In *Proceeding of IEEE Radar Conference*, May 2008.

[19] Willis, N.
Bistatic Radar (2nd ed.).
Raleigh, NC: SciTech Publishing, 2005.

[20] Varshney, P.
Distributed Detection and Data Fusion.
New York: Springer-Verlag, 1996.

[21] Wicks, M.
Space-time adaptive processing: A knowledge-based perspective for airborne radar.
IEEE Signal Processing Magazine, **23**, 1 (Jan. 2006), 51–65.

[22] Ali, M. and Obaidullah, M.
Distribution of linear combination of exponential variates.
Communications in Statistics—Theory and Methods, **11**, 13 (1982), 1453–1463.

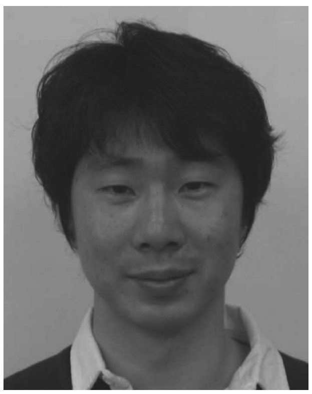

Byung Wook Jung (S'06) was born in Seoul, Korea. He received B.S. in electrical engineering from the University of Seoul in 2004. He is currently working toward the Ph.D. degree at Korea Advanced Institute of Science and Technology (KAIST), Daejeon, Korea.

His research interests include signal processing algorithm for distributed radar systems and global optimization.

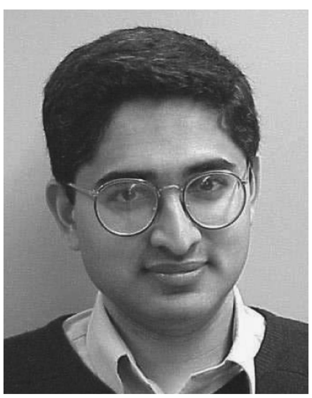

Raviraj Adve (S'88—M'97—SM'06) was born in Bombay, India. He received his B.Tech. in electrical engineering from IIT, Bombay, in 1990 and his Ph.D. from Syracuse University, Syracuse, NY, in 1996.

Between 1997 and August 2000, he worked for Research Associates for Defense Conversion Inc. on contract with the Air Force Research Laboratory at Rome, NY. He joined the faculty at the University of Toronto in August 2000 where he is currently an associate professor. His research interests include practical signal processing algorithms for multiple input multiple output (MIMO) wireless communications and distributed radar systems.

Dr. Adve received the 2009 Fred Nathanson Young Radar Engineer of the Year award.

Joohwan Chun (S'82—M'94—SM'09) received his Ph.D. degree from Stanford University, Stanford, CA, in 1989.

From 1989 to 1992, he was a member of the technical staff at General Electric, Schenectady, NY. Since 1992 he has been a faculty member in the Department of Electrical Engineering at Korean Advanced Institute of Science and Technology (KAIST). He was a visiting professor at Stanford University in 1998–1999. His fields of interest include the detection and estimation theory and wireless communications.

Michael C. Wicks (S'81—M'81—SM'90—F'98) received the B.S. degree in electrical engineering from the Rensselaer Polytechnic Institute, Troy, NY, in 1981 and the M.S. and Ph.D. degrees in electrical engineering from Syracuse University, Syracuse, NY, in 1985 and 1995, respectively.

He is the senior scientist for Sensor Signal Processing, Sensors Directorate, Air Force Research Laboratory, Rome, NY, specializing in the science and technology needed for superior U.S. air and space systems for reconnaissance, surveillance, precision engagement, and electronic warfare. He began his career with the Air Force in 1981, advanced to senior engineer by 1990, principal engineer by 1998, and assumed his current position in 2002. His technical expertise encompasses space-time adaptive processing, advanced algorithm development, and ultrawideband radar. His expertise includes polarimetric sensor signal processing, inverse synthetic aperture radar imaging, knowledge-based applications to radar signal processing, concealed weapons detection, ground-penetrating radar, bistatic radar, and radar systems engineering.

Dr. Wicks holds 14 U.S. patents (with a 15th patent pending), and has authored or coauthored two books, several book chapters, and over 300 journal, conference, and technical papers. He participates in numerous national and international panels, committees, and working groups, including NATO and other multinational organizations. He received the IEEE Fred Nathanson Memorial Award for the Young Engineer of the Year in 1998 and the IEEE Warren D. White Award for Excellence in Radar Engineering in 2009.